Received: 05 September 2015 | Accepted: 22 March 2017

DOI: 10.1111/gbi.12241

ORIGINAL ARTICLE

WILEY gebiology

Microbial acceleration of aerobic pyrite oxidation at circumneutral pH

E. Percak-Dennett[1] | S. He[1] | B. Converse[1] | H. Konishi[1] | H. Xu[1] | A. Corcoran[2] | D. Noguera[2] | C. Chan[3] | A. Bhayyacharyya[4] | T. Borch[4] | E. Boyd[5] | E. E. Roden[1]

[1]Department of Geoscience, NASA Astrobiology Institute, University of Wisconsin-Madison, Madison, WI, USA

[2]Department of Civil and Environmental Engineering, University of Wisconsin-Madison, Madison, WI, USA

[3]Department of Geological Sciences, University of Delaware, Newark, DE, USA

[4]Department of Soil and Crop Sciences, Colorado State University, Fort Collins, CO, USA

[5]Department of Microbiology & Immunology, Montana State University, Bozeman, MT, USA

Correspondence
E. E. Roden, Department of Geoscience, NASA Astrobiology Institute, University of Wisconsin-Madison, Madison, WI, USA.
Email: eroden@geology.wisc.edu

Funding information
NASA Astrobiology Institute; U.S. Department of Energy; Office of Biological and Environmental Research; Pacific Northwest National Laboratory (PNNL); University of Wisconsin-Madison

Abstract

Pyrite (FeS_2) is the most abundant sulfide mineral on Earth and represents a significant reservoir of reduced iron and sulfur both today and in the geologic past. In modern environments, oxidative transformations of pyrite and other metal sulfides play a key role in terrestrial element partitioning with broad impacts to contaminant mobility and the formation of acid mine drainage systems. Although the role of aerobic micro-organisms in pyrite oxidation under acidic-pH conditions is well known, to date there is very little known about the capacity for aerobic micro-organisms to oxidize pyrite at circumneutral pH. Here, we describe two enrichment cultures, obtained from pyrite-bearing subsurface sediments, that were capable of sustained cell growth linked to pyrite oxidation and sulfate generation at neutral pH. The cultures were dominated by two *Rhizobiales* species (*Bradyrhizobium* sp. and *Mesorhizobium* sp.) and a *Ralstonia* species. Shotgun metagenomic sequencing and genome reconstruction indicated the presence of Fe and S oxidation pathways in these organisms, and the presence of a complete Calvin–Benson–Bassham CO_2 fixation system in the *Bradyrhizobium* sp. Oxidation of pyrite resulted in thin (30–50 nm) coatings of amorphous Fe(III) oxide on the pyrite surface, with no other secondary Fe or S phases detected by electron microscopy or X-ray absorption spectroscopy. Rates of microbial pyrite oxidation were approximately one order of magnitude higher than abiotic rates. These results demonstrate the ability of aerobic microbial activity to accelerate pyrite oxidation and expand the potential contribution of micro-organisms to continental sulfide mineral weathering around the time of the Great Oxidation Event to include neutral-pH environments. In addition, our findings have direct implications for the geochemistry of modern sedimentary environments, including stimulation of the early stages of acid mine drainage formation and mobilization of pyrite-associated metals.

1 | INTRODUCTION

Pyrite (FeS_2) is the most abundant sulfide mineral on Earth, and its oxidation through biotic and abiotic pathways is a major source of sulfate input to oceans both in modern (Berner & Berner, 1996; Raymond & Oh, 2009) and ancient environments (Crowe et al., 2013; Konhauser et al., 2011; Stueken, Catling, & Buick, 2012). Oxidative transformation of pyrite and other metal sulfides plays a key role in terrestrial element partitioning with broad impacts to contaminant mobility and the formation of acid mine drainage systems (Schippers, 2004). Microbial pyrite oxidation has been extensively studied at low pH, mainly in the context of acid mine/rock drainage. Under acidic conditions, microbial catalysis greatly accelerates pyrite oxidation through aerobic oxidation of soluble Fe^{2+}, which produces Fe^{3+} ions that serve as an effective

chemical oxidant for FeS_2. However, many soil and sediment environments are not acidic but rather have a circumneutral pH, where pyrite oxidation can occur abiotically through reaction with atmospheric O_2 (Moses & Herman, 1991), or potentially through biologically catalyzed pathways.

Recent work has provided evidence for anaerobic nitrate-dependent pyrite oxidation under circumneutral-pH conditions in both field and laboratory settings (see Bosch and Meckenstock (2012) for a review). By comparison there is much less information on the potential for aerobic microbial oxidation of pyrite at circumneutral pH, even though the potential metabolic energy yield of this process is greater than that for nitrate-dependent oxidation. An early study of chemolithotrophic microbial metabolism in hydrothermal vent systems reported growth of aerobic micro-organisms on ground commercial pyrite as well as pyrite-bearing vent materials (Wirsen, Jannasch, & Molyneaux, 1993). In this work utilization of pyrite (and other reduced S compounds) as an energy source for growth was inferred from incorporation of $^{14}CO_2$ into cell biomass. Similar results were reported in a subsequent study with a pure *Thiomicrospira* isolate from vent materials (Wirsen et al., 1998). Employing analogous methods, Edwards, Rogers, Wirsen, and Mccollom (2003), demonstrated modest levels of cell growth and inorganic carbon fixation by a marine *Gammaproteobacterial* isolate (strain FO10) in seawater medium containing ground specimen pyrite. Unfortunately, none of these studies documented microbe–mineral associations or generation of sulfate or other oxidized S products during cell growth. Mielke, Pace, Porter, and Southam (2003) showed that the acidophilic Fe(II)-oxidizing bacterium *Acidithiobacillus ferrooxidans* colonized cubes of specimen pyrite at pH values of 6.5–6.7, but did not provide chemical evidence for major oxidative transformation of the mineral. Rhine, Onesios, Serfes, Reinfelder, and Young (2008) documented stoichiometric release of sulfate and arsenate during biologically accelerated oxidation of arsenopyrite at circumneutral pH and reported (but did not show) similar results for pyrite. This latter study provides the most convincing evidence to date for the ability of aerobic micro-organisms to accelerate pyrite oxidation under neutral-pH conditions.

With the exception of the above-mentioned studies, it appears that most investigators have assumed that abiotic reaction with O_2 dominates pyrite oxidation under neutral-pH conditions, where the solubility of Fe^{3+} is too low to permit rapid coupled biotic/abiotic oxidation of FeS_2 based on aqueous Fe redox cycling (Singer & Stumm, 1970). Nevertheless, aerobic microbial colonization and biological oxidation of pyrite under neutral-pH conditions has the potential to play a key role in the early stages of acid mine/rock drainage formation (Mielke et al., 2003). In fact, Mielke et al. (2003) concluded that the observed colonization of pyrite by *A. ferrooxidans* was facilitated by the development of an acidic nanoenvironment between the bacteria and the mineral surface, which in due course would lead to acidification of the bulk environment. In addition to contributing to the incipient development of acid mine/rock drainage conditions, a recent series of microbiological and geochemical studies (Boyd, Hamilton, Havig, Skidmore, & Shock, 2014; Hamilton, Peters, Skidmore, & Boyd, 2013; Harrold et al., 2016; Mitchell, Lafreniere, Skidmore, & Boyd, 2013) suggest the existence of neutral-pH aerobic, microbially mediated pyrite oxidation activity in well-buffered, pyrite-containing subglacial carbonate sediments.

This study investigated the ability of bacteria from a subsurface redox transition zone (located at the Hanford 300 Area in Eastern Washington) to oxidize synthetic framboidal pyrite under aerobic, neutral-pH conditions. Two enrichment cultures (T26 and R31) demonstrated sustained sulfate production and cell growth in medium where pyrite was the sole energy source during 12 successive transfers over a period of 350 days. Rates of pyrite oxidation, changes to pyrite framboids, cell–mineral associations, and composition of microbial communities were monitored during oxidation. A metagenomic analysis of organisms in the cultures was conducted to gain insight into potential mechanisms of microbially accelerated pyrite oxidation. Our results document the ability of bacteria to accelerate aerobic pyrite oxidation at neutral pH, a novel chemolithotrophic process with potentially broad environmental impacts and implications for sulfur and iron cycling on both modern and ancient Earth.

2 | MATERIALS AND METHODS

2.1 | Microbial culturing

2.1.1 | Enrichment culturing

Subsurface sediment was recovered from the Department of Energy's (DOE's) Hanford 300 Area Integrated Field Research Challenge (IFRC) site (http://ifchanford.pnl.gov), borehole 399-2-25, well IC C7870 (Bjornstad, Horner, Vermeul, Lanigan, & Thorne, 2009) in March 2011. The sediment was obtained under sterile conditions, and stored anoxically at 4°C prior to use as an inoculum for enrichment cultures (see Percak-Dennett and Roden (2014) for a full description of these experiments). Material from a redox transition zone at 17.8 m depth (Lin et al., 2012; Percak-Dennett & Roden, 2014; Peretyazhko et al., 2012) was used as inoculum for culture T26, and reduced material from 19 m depth was the source of inoculum for culture R31; each inoculum source was used to initiate duplicate enrichments. In addition to inoculation material, the initial enrichment cultures also contained (5 g per 100 ml fluid) of anoxically dried, ground and sieved reduced sediment. Sediment was not added in any subsequent culture transfers.

All cultures were grown in stoppered/crimp-sealed bottles with an air headspace to maintain aerobic conditions. The culture medium contained 10 mM l-1 piperazine-N,N-bis-2-ethanesulfonic acid (PIPES), 0.345 mM KH_2PO_4, 1.3 mM KCl, and 1 ml per liter of a vitamin and trace element solution (Lovley, 1987). Pyrite was added to enrichment cultures to a final concentration of ca. 20 mmol/L (ca. 40 mmol S/L). No organic carbon was present in the medium, and fixed nitrogen (e.g., ammonium) was also excluded to prevent the growth of nitrifiers. All cultures were incubated at room temperature in the dark. Duplicate sterile (autoclaved) controls were treated identically to inoculated reactors. The pH of the medium remained constant at 6.8 ± 0.3 for the duration of all experiments.

Synthetic framboidal pyrite was synthesized as previously described (Berner, 1969; Sweeney & Kaplan, 1973). After synthesis, pyrite was washed with 6M HCl and acetone to remove iron monosulfide (FeS) and elemental S (S^0) contaminants. However, X-ray diffraction (XRD) analysis revealed that a minor amount of S^0 was still present (Fig. S1), and additional washings were necessary to remove all S^0. XRD showed that the final mineral preparation was free of S^0 and composed of pyrite together with small quantities of its polymorph marcasite (Fig. S1). The material was suspended in anoxic distilled water to a concentration of ca. 1 mol/L and autoclaved. Pyrite framboids were digested in concentrated HNO_3 and the Fe content determined using ferrozine (Stookey, 1970). The sulfur content of the pyrite was measured via a single-step chromium reduction assay (Fossing & Jorgensen, 1989) with colorimetric sulfide determination (Cline, 1969). The results were consistent with the 1:2 Fe:S ratio expected for pyrite. Scanning electron microscopic (SEM) analysis of anoxically dried pyrite revealed that the μm-sized framboids consisted of aggregates of much smaller (5–10 nm) crystallites (Fig. S2). The measured BET surface area of the dried pyrite was 1.03 m^2/g.

After inoculation, samples were collected aseptically (via syringe and needle) from each culture every 7–21 days. The suspensions were microcentrifuged and the supernatant diluted 1:20 for sulfate measurement using ion chromatography (IC, Dionex Model ICS-1100). The initial enrichment cultures were grown for ca. 100 days prior to transfer, at which point all cultures and sterile controls were transferred (10% vol/vol of both liquid and solids) to fresh pyrite-containing medium. In all subsequent generations, transfers were made when the sulfate concentration in any individual culture was ≥2 mM.

2.1.2 | Growth experiments

The ninth transfer of the cultures was monitored for a longer time frame (79 days), and additional measurements were made to characterize the pyrite oxidation process. In addition to monitoring sulfate concentration, total polythionate concentrations were determined using the colorimetric procedure of Kelly and Wood (1994). The solids were subjected to a 1-hr extraction with 1M HCl, which liberated ~10% of total Fe in pyrite (data not shown) and was used to monitor changes in Fe redox speciation during pyrite oxidation. Cell–mineral associations were examined in fresh culture samples by SYTO® Green staining and epifluorescence microscopy as previously described (Emerson et al., 2007). For cell counts, subsamples were fixed with glutaraldehyde and immediately frozen at −80°C. Cell counts were made for days 0, 14, 34, and 54 by 4′,6-diamidino-2-phenylindole (DAPI) staining and epifluorescence microscopy following established protocols (Hobbie, Daley, & Jasper, 1977). Fluorescence in situ hybridization (FISH) was completed on cells from day 54 using primers Bet42a (Betaproteobacteria), Alfa968 (Alphaproteobacteria), and Eub338 (most Bacteria) following established protocols (Hugenholtz, Tyson, & Blackall, 2002). Visualization of hybridized cells was carried out on a Zeiss Axio Imager 2 (Zeiss, Oberkochen, Germany). Additional subsamples were centrifuged, rinsed with distilled water, and dried anoxically for TEM, SEM, and XRD analysis. Also at day 54, subsamples were obtained for DNA extraction and cryo-SEM imaging. Samples used for DNA extraction were immediately frozen at −80°C.

2.2 | Characterization of solid phases

2.2.1 | X-ray diffraction and electron microscopy

Dried, unaltered pyrite grains were examined using a Rigaku Rapid II XRD and Hitachi S-3400 variable pressure SEM (Madison WI). Dried, unaltered and microbially oxidized pyrite grains were examined with a FEI Titan Aberration Corrected scanning/transmission electron microscope (Madison WI) as previously described (Shelobolina et al., 2012b). Culture samples for cryo-SEM imaging were used immediately; the samples were mounted on a polycarbonate filter, and plunged into liquid nitrogen slush. A vacuum was pulled allowing sample transfer to the Gatan Alto 2500 cryo chamber at a temperature of 120°C. Samples were then sublimated for 10 min at 90°C followed by cooling to 120°C. A thin layer of gold–palladium was sputtered onto the samples, after which they were transferred into a Hitachi S-4700 field-emission scanning electron microscope for imaging.

2.2.2 | X-ray absorption spectroscopy

Fe and S speciation (oxidation state and chemical coordination environment) were determined using X-ray absorption spectroscopy (XAS) analyses. Fe K-edge extended X-ray absorption fine structure (EXAFS) (7112 eV) and S K-edge X-ray absorption near-edge structure (XANES) (2472 eV) spectral analysis were conducted on beamline 4-3 at the Stanford Synchrotron Radiation Laboratory (SSRL), at Menlo Park, CA, under ring operating conditions of 3 GeV with a current of 450 mA. Samples were sealed on Teflon holders with Kapton tape to preserve the oxidation state of Fe and S and to prevent from any potential beam damage which might occur during data collection. A double crystal Si (220) monochromator with an unfocused beam was detuned 30% to reject harmonics affecting the primary beam. Between 7 and 10 individual spectra were averaged for each sample. Pure elemental Fe foil was used for energy calibration for Fe at 7112 eV whereas thiosulfate ($S_2O_3^{2-}$) was used for energy calibration of S at 2472 eV. The Lytle detector was used to record the fluorescence spectra of EXAFS and XANES scans. The fluorescence spectra were averaged and pre- and post-edge subtracted using Athena (Ravel & Newville, 2005). Linear combination fitting (LCF) of k^3-weighted Fe K-edge EXAFS was also performed using Athena to identify potential Fe-bearing phases in the samples (Ravel & Newville, 2005). LCF of spectra was performed in k^3-weighted k-space between k = 2 and 14, using the following end-members: siderite ($FeCO_3$), 2- and 6-line ferrihydrite [$Fe(OH)_3$ nH_2O], goethite (α-FeOOH), lepidocrocite (γ-FeOOH), hematite (α-Fe_2O_3), green rust ($Fe^{II}_{6x}Fe^{III}_x[OH]_{12}[(SO_4)_{x/2}$ $3H_2O]$), pyrite (FeS_2), mackinawite (FeS), and magnetite (Fe_3O_4). These references were chosen based on their likelihood to be present under experimental conditions. Compounds were only included in the fit if the contribution was a fraction greater than 0.05. The oxidation states of S in the samples were identified by comparing the maximum energies of the spectra with that of oxidized S (sulfate; S in +6 oxidation state).

TABLE 1 Draft genomes recovered from the four most abundant organisms in culture T26

Classification of 16S rRNA sequence using RDP classifier[a]	Best BLASTn hit of 16S rRNA sequence against NCBI nr[b]	Classification of essential single-copy genes by MEGAN[c]	Total base pair in draft genome (Mbp)	Estimated genome completeness[d] (%)	Average fold coverage of contigs (X)	GC content (%)
Bradyrhizobium (97%)	*Bradyrhizobium* (99%)	*Bradyrhizobiaceae*	6.52	97	511	67.3
Chitinophagaceae (100%)	*Sediminibacterium* (99%)	*Chitinophagaceae*	3.40	96	624	37.4
Ralstonia (100%)	*Ralstonia* (100%)	*Ralstonia*	5.66	92	40	63.5
Hyphomicrobium (100%)	*Hyphomicrobium* (99%)	*Hyphomicrobium*	4.55	81	62	60.5

[a]16S rRNA gene sequences in the draft genomes were classified by RDP classifier (http://rdp.cme.msu.edu), and the values in parentheses indicate confidence levels of classification.
[b]Best BLASTn hits of 16S rRNA gene sequences in the draft genomes against the NCBI nr database, and the values in parentheses indicate percent identities.
[c]Classification of essential single-copy genes in draft genomes is based on the consensus (i.e., the majority) of their taxonomic assignments by MEGAN (Huson & Weber, 2013) using BLASTp hits.
[d]The genome completeness was estimated by dividing the number of essential single-copy genes recovered in each draft genome by the expected number of these genes in a complete genome.

2.3 | Microbial community analysis

2.3.1 | 16S rRNA gene clone libraries

DNA was extracted from frozen culture samples with a Mo-Bio PowerSoil® DNA Isolation kit with some modifications. Frozen cultures were thawed, added to bead-beating tubes with 80 µl solution C1. The samples were then heated at 60°C for 10 min with vigorous shaking at 14,000 rpm using an Eppendorf Thermomixer. After this, the manufacturer's recommended procedure was followed. Near full length 16S rRNA gene clone libraries were constructed using primers GM3 and GM4R (Muyzer, Teske, Wirsen, & Jannasch, 1995) as previously described (Roden et al., 2012). Clones were constructed using the pGEM-T vector and *Escherichia coli* JM109 competent cells (Promega). Sanger 16S rRNA gene sequences of recombinant transformants were obtained from the University of Wisconsin-Madison Biotechnology Center. Assembled clones were screened for chimeras using UCHIME (Edgar, Haas, Clemente, Quince, & Knight, 2011) and flagged sequences were subsequently examined in Pintail (Ashelford, Chuzhanova, Fry, Jones, & Weightman, 2005). Suspicious sequences were excluded from downstream analysis. The 16S rRNA gene sequences were submitted to BLAST for taxonomic identification, using the BLASTn algorithm with environmental sequences excluded from the database (Altschul et al., 1997). Representative sequences and their taxonomic assignments are available in GenBank under accession numbers KX779309–KX779316.

2.3.2 | Shotgun metagenomic analysis

A shotgun Illumina library (insert sizes of ca. 280–320 bp) was constructed from Culture T26 genomic DNA and sequenced on the Illumina HiSeq 2000 platform to generate paired-end (2 × 100 bp) reads. A total of 8.4 Gbp of sequences were generated. Metagenome assembly was performed using CLC Genomic Workbench (version 6, CLC bio Inc., Cambridge, Massachusetts, USA). Briefly, raw reads were quality-trimmed and length-filtered, and assembled with an automatically estimated k-mer by CLC Genomic Workbench with scaffolding. The average coverage of each contig was estimated by mapping QC-ed reads back to the contigs using CLC Genomic Workbench. By checking the contig coverage consistency, two chimeric joints were identified and manually corrected. All contigs were uploaded to the Integrated Microbial Genomes with Microbiomes (IMG/M) database (img.jgi.doe.gov/m) for gene prediction and functional annotation (Markowitz et al., 2014), and are available under IMG/M Taxon ID of 3300001911.

Protein coding genes were searched against the hidden Markov models (HMMs) constructed for 107 proteins which are conserved in 95% of all sequenced bacteria (Dupont et al., 2012), by performing hmmsearch (HMMER 3.0.) to identify essential single-copy genes as described in Albertsen et al. (2013). Identified essential deduced protein sequences were searched against the NCBI refseq_protein database by BLASTP, and the BLAST output was imported to MEGAN (Huson & Weber, 2013) for taxonomic assignments using the lowest common ancestor algorithm, as described in Albertsen et al. (2013). Essential genes assigned to the same taxonomic group were on contigs with comparable coverage, indicating that they indeed belong to the same organism. The analysis of essential single-copy genes clearly suggested four major organism bins. Taxonomic binning was performed on contigs longer than 1 kbp using a combination of GC content, contig coverage (indicative of organism abundance), and sequence homology. For sequence homology, all protein sequences were searched against the NCBI refseq_protein database by BLASTp and assigned to taxa by MEGAN. The consensus taxa inferred from all proteins in a contig was used to indicate the contig's putative taxonomy to facilitate its binning in combination with GC content and contig coverage. To verify binning results, tetranucleotide frequencies generated from all contigs longer than 3 kbp were analyzed using an emergent self-organizing map (ESOM) (Dick et al., 2009), and the clustering pattern on ESOM indicates that binning is accurate. Partial- to complete-length 16S rRNA gene sequences were recovered within each bin. Their classifications by RDP classifier and the best BLASTn hits against the NCBI nr database were both consistent with the taxonomic assignment of the essential single-copy genes (Table 1). These results suggested the recovery of 4 draft

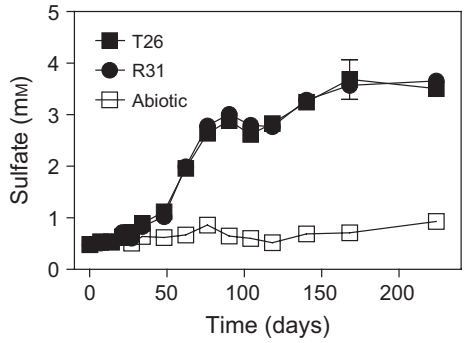

FIGURE 1 Sulfate production in the initial enrichment cultures in comparison with abiotic control. Each data point represents the mean ± range of duplicate cultures for T26 and R31 and a single uninoculated control

genomes, and the genome completeness was estimated by dividing the number of essential single-copy genes recovered from each draft genome by the expected number (107) of these genes in a complete genome (Albertsen et al., 2013). The four draft genomes are available at the U.S. Department of Energy, Joint Genome Institute IMG/M data portal with Taxon IDs of 2654587905-2654587908.

3 | RESULTS

3.1 | Microbially mediated pyrite oxidation

After a ca. 30 day lag period, sulfate began to accumulate in the initial enrichment cultures, increasing to 3.5 mM over a ca. 200 day period (Figure 1). Uninoculated treatments showed a much smaller increase in sulfate (ca. 0.5 mM) over the same time period. After 150 days, the initial enrichment cultures were transferred to fresh medium containing ca. 20 mmol/L of pyrite. Generation of ca. 4 mM sulfate was observed within 14 days of transfer, at which time all cultures and sterile controls were transferred again. Sulfate concentrations in inoculated cultures again increased to ca. 4 mM after another 14 days, and all cultures were subsequently transferred. For 280 days, rapid generation of 3–4 mM sulfate occurred within 14–28 days after transfer for all inoculated cultures (Figure 2). Uninoculated controls showed <0.5 mM sulfate generation during each successive transfer. pH values were monitored periodically and remained between 6.8 and 7.1. Concentrations of sulfate produced during the first 10 transfers (241 days), together with the measured BET surface area of the particles (ca. 1 m^2/g), were used to calculate surface area-normalized rates of sulfate production (Fig. S3). Sulfate production for both cultures (T26 and R31) averaged $1.91 \pm 1.29 \times 10^{-9}$ mol m^{-2} s^{-1}, an order of magnitude higher than abiological rates which averaged $3.15 \pm 3.24 \times 10^{-10}$ mol m^{-2} s^{-1}. The observed abiotic surface area-normalized rates are comparable to previously determined rates of chemical oxidation of ca. 40 µm sized particles of specimen pyrite by O_2 at circumneutral pH (Moses & Herman, 1991), but ca. 10-fold higher than rates of sub-µm sized synthetic pyrite oxidation in seawater (Gartman & Luther, 2014).

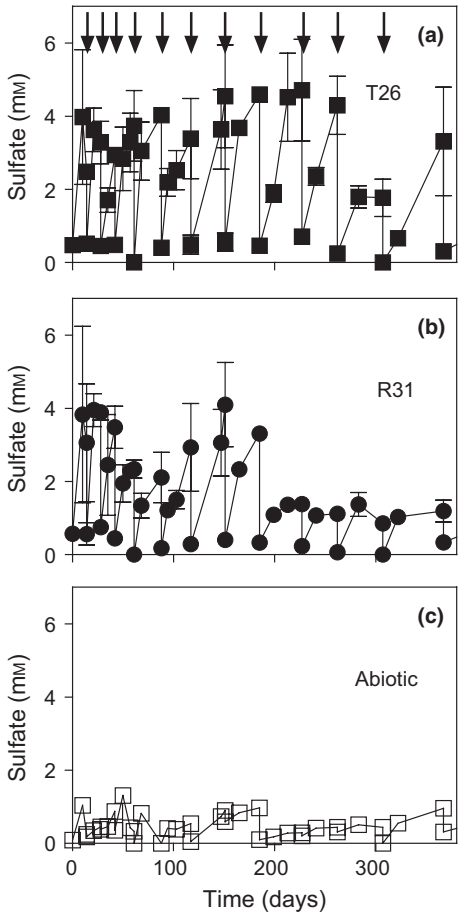

FIGURE 2 Sulfate production during 11 successive transfers of the enrichment cultures T26 and R31 (a and b) in comparison with abiotic control (c). Arrows in panel a indicate culture transfers. Each data point represents the mean ± range of duplicate cultures for T26 and R31 and a single uninoculated control

The ninth generation of the cultures was monitored in detail to link mineral alteration and cell growth to pyrite oxidation. Approximately 6 mM of sulfate was generated over a 76 day period, compared to ca. 3 mM in uninoculated controls (Figure 3a). These levels of sulfate production correspond to oxidation of ca. 15% and 7.5% of pyrite-S, respectively. Total polythionate concentrations were slightly lower initially in inoculated compared to abiotic cultures (Figure 3b), and both systems showed a gradual decrease in polythionates over time. HCl-extractable Fe(II) initially accounted for ca. 10% of pyrite-Fe, and was expressed as the ratio of Fe(II) to total Fe in the extract to assess Fe(II) loss during oxidation. The relative abundance of Fe(II) decreased by a factor of 3 during the experiment (Figure 3c), with the rate of Fe(II) loss being more rapid in the inoculated cultures compared to abiotic controls.

Direct cell counts on the ninth generation cultures revealed a 3-fold increase in cell density between day 0 and day 54, with the number of cells doubling by day 14 and final cell concentration reaching ca. 5×10^7 cells/ml (data not shown). No cells were observed in abiotic controls. SYTO Green DNA staining of fresh culture samples revealed that virtually all cells were directly associated with mineral surfaces (Figure 4a, b). Cryo-SEM analysis confirmed a close spatial

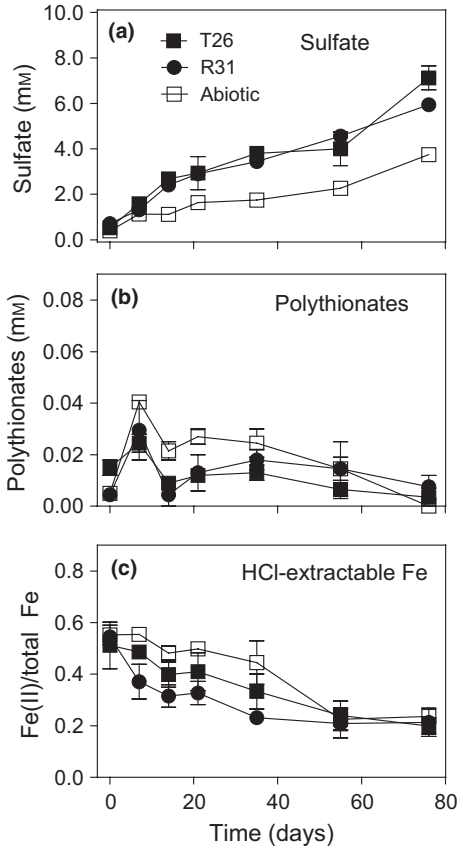

FIGURE 3 Changes in sulfate (a), total polythionates (b) and HCl-extractable Fe(II) (c) during the ninth generation of the enrichment cultures in comparison with abiotic control. Each data point represents the mean ± range of duplicate cultures for T26 and R31 and a single abiotic control

relationship between pyrite framboids and microbial cells with very few unattached cells (Figure 4c, d).

3.2 | Mineralogical alteration of pyrite framboids

XRD analysis of solids from the ninth transfer showed no major changes to pyrite crystalline structure and an absence of secondary minerals such as Fe(III) oxides (data not shown). However, linear combination fit analyses of Fe K-edge EXAFS spectra showed increased concentrations of ferrihydrite and decreased FeS_2 concentrations in oxidized pyrite (Fig. S4). No distinct S-bearing mineral phases were detected by SEM, TEM, or XRD. S K-edge XANES indicated the absence of S in anything other than the −2 oxidation state (Fig. S5). These results, together with the fact that no distinct S-bearing mineral phases were detected by TEM, indicated complete oxidation of FeS_2 to sulfate and amorphous Fe(III) oxide (ferrihydrite). Consistent with this interpretation, TEM analysis of solids from the ninth transfer revealed thin (30–50 nm) amorphous coatings on oxidized framboids (Figure 5a), which were not evident on unreacted materials (Figure 5b). Although these results show convincingly that reduced S intermediates were not present at the end of the experiment shown in Figure 3, we cannot rule out the possibility that such intermediates were present earlier in the experiment.

3.3 | Microbial community analysis

The taxonomic composition of the enrichment culture clone library sequences (n = 85 and 75 for T26 and R31, respectively) indicated microbial communities (Table S1) dominated by *Alphaproteobacteria* from the family *Bradyrhizobiaceae* (*Bradyrhizobium* and *Mesorhizobium*

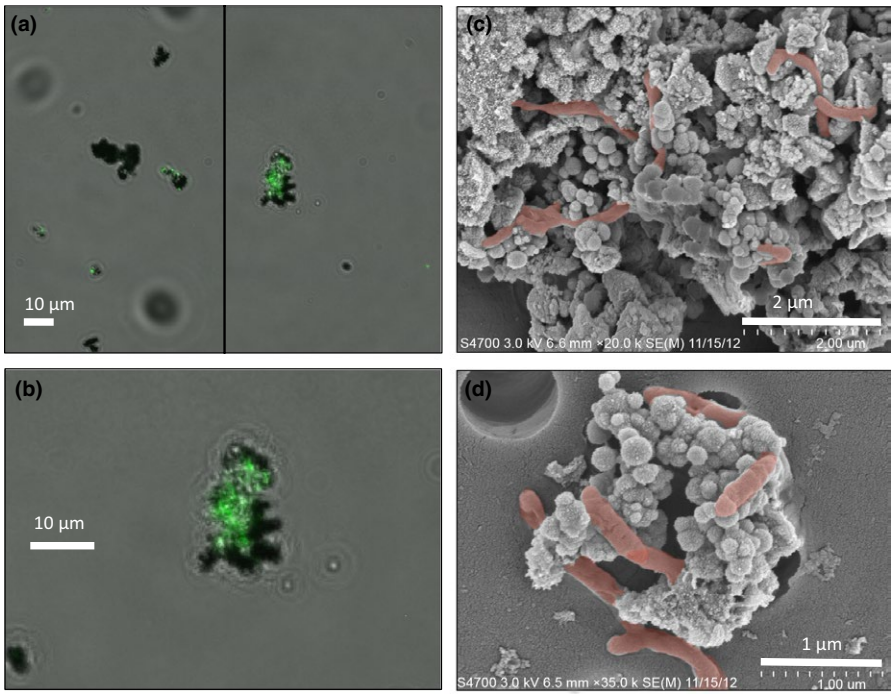

FIGURE 4 SYTO green DNA stain (a, b) and cryo-SEM images of the ninth generation of enrichment culture R31 after ca. 45 days of growth. Panel a shows two different microscopic fields; panel b shows an enlargement of the large cell–mineral association shown in panel a. Cells are shown in false orange color in panels c and d

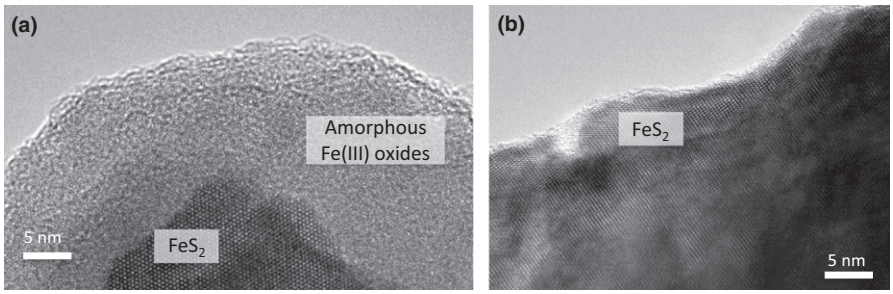

FIGURE 5 TEM images of microbially altered (culture R31) (a) and unaltered (b) pyrite framboids. The microbially altered minerals display a thin (30–50 nm) coating of amorphous Fe(III) oxides on framboids. No distinct S-bearing mineral phases were detected

sp.), and the betaproteobacterial genus *Ralstonia*, as well as the sphingobacterial genus *Sediminibacterium*. FISH analysis indicated that the attached microbial communities were dominated by *Alphaproteobacteria* (Fig. S6) with much lower abundance of *Betaproteobacteria* (data not shown).

Taxonomic binning and ESOM analysis of the T26 metagenome yielded draft genomes from four dominant organisms (Figure 6), which were classified to the genera *Bradyrhizobium*, *Ralstonia*, *Hyphomicrobium*, and the family *Chitinophagaceae*, with estimated genome completeness of 97%, 92%, 81%, and 96%, respectively (Table 1). The *Ralstonia* sp. 16S rRNA gene sequence recovered from the metagenome matched 35 sequences in the T26 clone library with >99% identity (0–3 mismatches), whereas the *Bradyrhizobium* sp. 16S rRNA gene in the metagenome matched 9 sequences from the T26 clone library with 97%–98% identity (12–18 mismatches). Therefore, the metagenome likely recovered the same *Ralstonia* sp. in the T26 clone library, along with a *Bradyrhizobium* sp. which was similar to but not identical to the *Bradyrhizobium* sp. in the clone library.

The reconstructed genome for *Bradyrhizobium* sp. contained complete pathways for autotrophic CO_2 fixation (Calvin–Benson–Bassham)) as well as a full complement of genes necessary for N_2 fixation (Fig. S7) via molybdenum nitrogenase (Boyd et al., 2011). Proliferation of a taxon with these capabilities was perhaps not unexpected given the absence of both fixed C and N in the enrichment culture medium. Homologues of sulfur-oxidizing *sox* genes (Friedrich, Rother, Bardischewsky, Quentmeier, & Fischer, 2001) were recovered in all community members except *Chitinophagaceae* sp., with *Bradyrhizobium* sp. and *Hyphomicrobium* sp. containing a complete *sox* pathway capable of thiosulfate oxidation to sulfate (Fig. S8). Several gene clusters potentially involved in extracellular electron transfer associated with Fe oxidation were recovered from the *Bradyrhizobium* sp., *Ralstonia* sp., and *Hyphomicrobium* sp. draft genomes (see Figure 7 and Discussion).

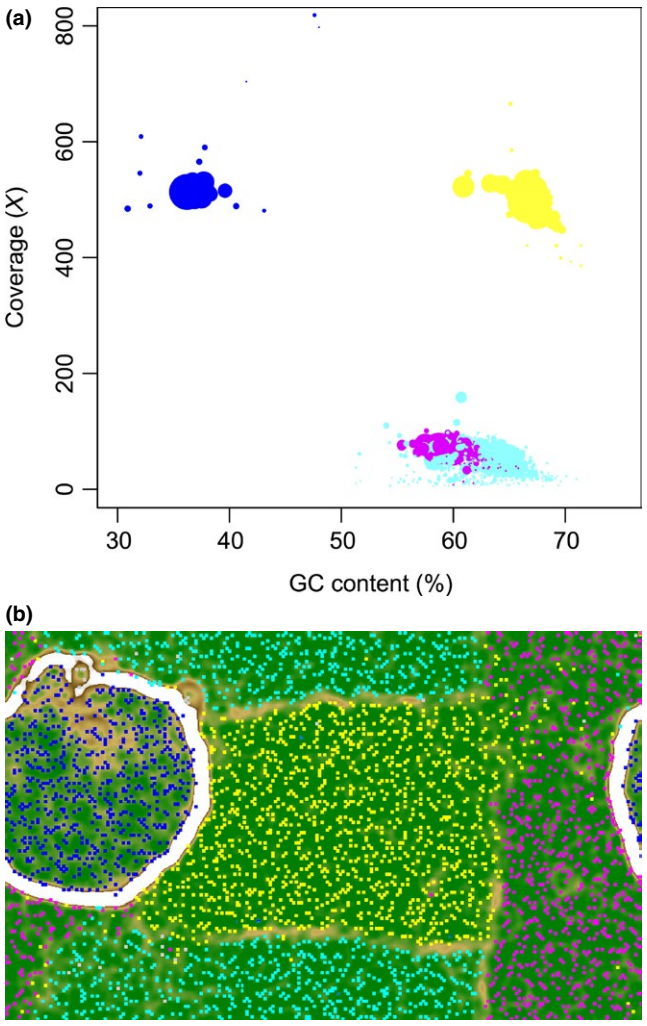

FIGURE 6 (a) Coverage vs. GC content for contigs (>1 kb length) from the T26 metagenome. Each symbol indicates a contig, and the size of each is scaled to the length of the contig. Taxonomic binning was based on the consensus result from contig coverage, GC content, and sequence similarity to reference genomes, and is indicated by different colors: ●*Bradyrhizobium*; ●*Hyphomicrobium*; ●*Chitinophagaceae*; ●*Ralstonia*. (b) Emergent self-organizing map (ESOM) of genomic sequence fragments from the T26 metagenome based on the tetranucleotide frequency calculated with a window size of 5 kbp. All contigs longer than 3 kbp were included in this analysis. Each dot represents a 5-kbp fragment (or the entire contig if its length is shorter than 5 kbp). Sequence fragments from different taxonomic bins are indicated by different colors (the same as in panel a)

4 | DISCUSSION

4.1 | Circumneutral-pH pyrite oxidation

Enhanced sulfate generation (relative to abiotic controls) over 12 transfers, increases in cell numbers, and the direct association between cells and pyrite framboids all indicate cell growth coupled to pyrite oxidation by organisms in the enrichment cultures. Sustained growth over 300 days indicates true chemolithoautotrophic growth as opposed to

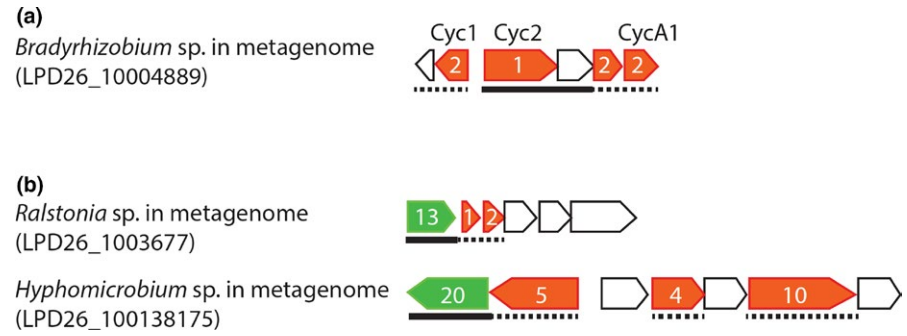

FIGURE 7 (a) The gene cluster including Cyc2, Cyc1, and CycA1 homologues of *Acidithiobacillus ferrooxidans*, with the Cyc2 gene locus tag labeled in the parenthesis. (b) Gene clusters including porin-like outer membrane protein- and periplasmic cytochrome *c*-encoding genes, with the porin-like gene locus tags labeled in the parentheses. Red arrows indicate genes encoding cytochrome *c*, and green arrows indicate genes encoding porin-like outer membrane protein. The number labeled in cytochrome *c* indicates the number of heme-binding sites, and the number labeled in porin-like OMP indicates the number of transmembrane motifs. Predicted cellular locations are indicated by different line types under the gene, with solid lines indicating outer membrane proteins and dash lines indicating periplasmic proteins

utilization of endogenous cellular reserves, which if present, would have been exhausted early in the experiment. The latter conclusion is supported by the presence of a complete Calvin–Benson–Bassham pathway for CO_2 fixation for the *Bradyrhizobium* sp. in the cultures, which presumably provided fixed carbon to heterotrophic organisms in the enrichments. The ability of heterotrophic bacteria to gain energy for growth from oxidation of reduced sulfur compounds (e.g., thiosulfate and other polythionates) while assimilating exogenous organic compounds is well known (e.g., Mason & Kelly, 1988; Sorokin & Lysenko, 1993; Trudinger, 1967; Tuttle, Holmes, & Jannasch, 1974; Tuttle & Jannasch, 1972), and in addition some reduced S-utilizing bacteria can fix significant quantities of CO_2 during mixotrophic growth (Sorokin, 1970; Sorokin & Lysenko, 1993; Tuttle & Jannasch, 1977, 1979; Zopfi, Ferdelman, Jorgensen, Teske, & Thamdrup, 2001). These observations provide an explanation for how pyrite was able to serve as the sole energy source for growth of mixed populations of autotrophic and mixotrophic bacteria in our enrichment cultures, as well as in previous studies with mixed and pure cultures of marine bacteria (Edwards et al., 2003; Wirsen et al., 1993, 1998).

The results of this study help to expand the known range of neutral-pH pyrite-oxidizing micro-organisms in aerobic terrestrial environments. To our knowledge the study by Rhine et al. (2008) represents the only prior demonstration of aerobic pyrite oxidation by micro-organisms from a neutral-pH terrestrial system, in this case a *Bosea thiooxidans* isolate (strain WAO) from arsenopyrite-bearing black shale in the Newark Basin near Trenton, NJ. In this context, it is interesting to consider whether or not the environment from which cultures T26 and R31 were obtained supports active aerobic and/or nitrate-dependent pyrite oxidation. The cultures were obtained from sediments either within (T26) or just below (R31) the subsurface redox transition zone (RTZ) within a fine-grained unit of the Ringold Formation at the Hanford 300 Area site in Eastern Washington (Lin et al., 2012; Percak-Dennett & Roden, 2014; Peretyazhko et al., 2012; Stegen et al., 2016). Reduced sediments from below the RTZ contain small (a few tens of μmols of reduced S per g) but detectable quantities of pyrite with framboidal textures (Peretyazhko et al., 2012). Sharp gradients in dissolved O_2 and nitrate are present within RTZ, with O_2 concentrations falling from near-saturation (ca. 250 μM) to zero between ca. 15 and 16 m depth, and nitrate concentrations falling from ca. 400 μM to zero between ca. 15.5 and 17.5 m depth (Lin et al., 2012). Interestingly, dissolved sulfate concentrations show two distinct step increases across these depth intervals, rising from ca. 450 to 560 μM in the first, and from ca. 560 to 800 μM in the second (see Figure 1 in Lin et al., 2012). These observations suggest that both aerobic and nitrate-linked pyrite oxidation may be taking place within this subsurface RTZ. Although controlled sediment incubation experiments failed to demonstrate aerobic or nitrate-dependent oxidation of endogenous pyrite (Percak-Dennett & Roden, 2014), the heterotrophic metabolism that dominated in those experiments may have been artificially stimulated as a result of disaggregation and dispersion of the Pliocene-age deposits (as observed previously in experiments with Cretaceous-age Atlantic Coastal Plain sediments, Chapelle & Lovley, 1990). Further studies of this and other analogous environments are required to assess the potential for aerobic and nitrate-driven pyrite oxidation across redox gradients in subsurface systems that contain authigenic pyrite from modern or ancient sulfate reduction activity.

4.2 | Mechanism(s) of microbial pyrite oxidation

By what mechanism(s) could micro-organisms from the RTZ enrichments have accelerated oxidative dissolution of pyrite? To address this question it is useful to consider established models for pyrite oxidation at acidic pH, for example, by organisms such as *A. ferrooxidans* and *Leptospirillum ferrooxidans* (Blake & Johnson, 2000). In the "indirect" mechanism for low-pH pyrite oxidation (Sand, Gehrke, Jozsa, & Schippers, 2001), enzymatic oxidation of aqueous Fe^{2+} (Table 2, reaction 1) results in the formation of Fe^{3+} ions that abiotically attack and dissolve the mineral, resulting in the release of sulfate and regeneration of aqueous Fe(II) (Table 2, reaction 2). Although this mechanism is not likely to be operative at circumneutral pH given the insolubility of Fe^{3+} at pH values greater than ca. 4 (Singer & Stumm, 1970), as discussed below the concept of a Fe-mediated mechanism cannot be ruled out solely on the basis of pH conditions.

TABLE 2 Reactions for pyrite oxidation mechanisms

Reaction	Mechanism
Low-pH, "soluble Fe redox cycling-based" model	
(1) $14Fe^{2+} + 3.5O_2 + 14H^+ \rightarrow 14Fe^{3+} + 7H_2O$	Enzymatic, may be promoted by cell-mineral contact
(2) $14Fe^{3+} + FeS_2 + 8H_2O \rightarrow 2\,SO_4^{2-} + 15Fe^{2+} + 16H^+$	Abiotic surface reaction
Net: $FeS_2 + 3.5O_2 + H_2O \rightarrow 2SO4^{2-} + Fe^{2+} + 2H^+$	
Circumneutral-pH, "polythionate (e.g., $S_2O_3^{2-}$) intermediate" model	
(3) $FeS_2 + 1.5O_2 \rightarrow S_2O_3^{2-} + Fe^{2+}$	Abiotic surface reaction
(4) $S_2O_3^{2-} + 2O_2 + H_2O \rightarrow 2SO4^{2-} + 2H^+$	Enzymatic, may be promoted by cell-mineral contact
(5) $Fe^{2+} + 0.25O_2 + 2.5H_2O \rightarrow Fe(OH)_3 + 2H^+$	Abiotic, may be enzymatically catalyzed
Net: $FeS_2 + 3.75O_2 + 3.5H_2O \rightarrow 2SO_4^{2-} + Fe(OH)_3 + 4H^+$	
Circumneutral-pH, "sorbed Fe redox cycling" model[a]	
(6) [b]$FeS_2 + Fe^{2+} \rightarrow FeS_2{\equiv}Fe(II)_{ads}$	Abiotic surface reaction
(7) $FeS_2{\equiv}Fe(II)_{ads} + 0.25O_2 \rightarrow FeS_2{\equiv}Fe(III)_{ads}$	Enzymatic, promoted by cell-mineral contact
(8) $FeS_2{\equiv}Fe(III)_{ads} \rightarrow FeSSOH{\equiv}Fe(II)_{ads}$	Abiotic (electron transfer from pyrite to $Fe(III)_{ads}$)
(9) $FeSSOH{\equiv}Fe(II)_{ads} + 0.25O_2 \rightarrow FeSSOH{\equiv}Fe(III)_{ads}$	Enzymatic, promoted by cell-mineral contact
(10) $FeSSOH{\equiv}Fe(III)_{ads} \rightarrow FeSSO_2H{\equiv}Fe(II)_{ads}$	Abiotic (electron transfer from pyrite to $Fe(III)_{ads}$)
(11) … $\rightarrow Fe(OH)_3 + 2SO_4^{2-}$	Multiple electron transfer steps, leading to formation of Fe(III) oxide and release of SO_4^{2-}
Net: $2FeS_2 + 3.75O_2 + 3.5H_2O \rightarrow 2SO_4^{2-} + Fe(OH)_3 + 4H^+$	

[a]Based on the model shown in Figure 9 in Moses and Herman (1991). For simplicity, H_2O and H^+ balance are omitted from all but the overall net reaction.
[b]The Fe^{2+} in this reaction may arise from the surface reaction of pyrite with O_2, for example, reaction 3.

A potential non-Fe-based indirect mechanism involves bacterial utilization of polythionate ions (e.g., thiosulfate, $S_2O_3^{2-}$) that are known to be released from the pyrite surface during abiotic reaction with O_2 at circumneutral pH (Moses, Nordstrom, Herman, & Mills, 1987) (Table 2, reaction 3). Bacterial utilization of $S_2O_3^{2-}$ (Table 2, reaction 4) would accelerate the conversion of pyrite-S to sulfate, given that rates of microbially mediated thiosulfate oxidation by O_2 are much faster than abiotic rates at circumneutral pH (Tuttle & Jannasch, 1976). Although oxidation of soluble Fe(II) produced during abiotic reaction of pyrite with O_2 (Table 2, reaction 5) could be biologically mediated (Emerson & Weiss, 2004), the results reported in Druschel et al. (2008) suggest that abiotic oxidation of Fe(II) by O_2 is likely to have dominated under the fully aerobic conditions in our cultures. Regardless of whether Fe(II) oxidation was abiotic or microbially mediated, at neutral pH any soluble Fe(II) produced would react quickly with O_2, resulting in formation of the Fe(III) oxide layer observed on the pyrite surfaces (Figure 5a). It should be noted here that thermodynamic calculations [made using ΔG_f values from Stumm and Morgan (1996) and Thauer, Jungermann, and Decker (1977)] show that the free energy release for the reaction (at pH 7):

$$FeS_2 + 1.75O_2 + 2.5H_2O \rightarrow S_2O_3^{2-} + Fe(OH)_3 + 2H^+$$

(which assumes rapid oxidation of Fe^{2+} produced via reaction 3 in Table 2 to amorphous Fe(III) oxide, $Fe(OH)_3$) is virtually unaffected by the assumed $S_2O_3^{2-}$ concentration; hence, any microbial acceleration of pyrite oxidation via thiosulfate scavenging would be due to a kinetic rather than a thermodynamic effect.

The fact that several organisms in the enrichment cultures contained the metabolic machinery (i.e., the *sox* system; see Supplementary Information) for polythionate oxidation (Figs. S7 and S8) is consistent with the above mechanism. In addition, the direct association of cells with the pyrite surface (Figure 4) suggests the possibility for an "indirect contact" mechanism akin to that known for acidophilic Fe(II)-oxidizing bacteria (Fowler, Holmes, & Crundwell, 2001; Sand et al., 2001), wherein mineral surface colonization results in Fe(II) oxidation and subsequent FeS_2 dissolution by Fe(III) ions within microenvironments at the cell–mineral interface. Recent dialysis bag experiments with a cold-adapted, thiosulfate-oxidizing *T. denitrificans* isolate (Harrold et al., 2016) have provided evidence that direct cell–mineral contact is required for aerobic microbial acceleration of pyrite oxidation (Boyd, Harrold, & Skidmore, 2016). Consistent with this observation, in situ mineral colonization studies conducted in the glacial outwash channel where this isolate was recovered found evidence for enrichment of 16S rRNA gene sequences affiliated with thiobacilli on FeS_2 surfaces when compared to silicate or carbonate surfaces (Mitchell et al., 2013).

Despite the fact that the *sox* system was likely operative to some extent in our cultures, the results of the polythionate measurements suggest that it may not have been the only, or even the dominant, mechanism for enhanced sulfate generation. Total polythionate concentrations were comparable in the abiotic versus biotic reactors

(Figure 3b), which would not be expected if mineral-associated bacteria thrived via scavenging of thiosulfate and other polythionates as they were released from the pyrite surface. Although these results by no means rule out a polythionate intermediate-based mechanism for microbially mediated pyrite oxidation, they motivate consideration of other possible mechanisms.

The work of Moses and Herman (1991) on abiotic reaction of pyrite with O_2 at neutral pH points toward a potential solid-phase Fe-based mechanism for microbial acceleration of pyrite oxidation in our cultures. That study concluded that the most likely mechanism for abiotic oxidation of pyrite-S to sulfate involved redox cycling of surface-associated Fe species. In this model (Table 2, reactions 6–11), Fe(II) (e.g., produced during the initial reaction of pyrite with O_2) undergoes adsorption to the mineral surface; the adsorbed Fe(II) then donates electrons to O_2, resulting in the formation of surface-associated Fe(III) that in turn rapidly accept electrons from reduced S in the underlying pyrite. Oxygen molecules are transferred from the hydration sphere of the adsorbed Fe to pyrite-S, and successive addition of oxygen continues until a stable sulfoxy species (e.g., sulfate) dissociates from the surface. Thus, in this model, cyclic oxidation and reduction of surface-associated Fe serves as a conduit for transfer of electrons from pyrite-S to dissolved O_2. Gartman and Luther (2014) reached similar conclusions regarding the mechanism of synthetic pyrite oxidation in seawater. Recent density functional theory/plane-wave calculations provide theoretical support for this basic mechanism (Dos Santos, Silva, & Duarte, 2016).

It seems feasible that mineral-associated bacterial cells could facilitate this process by accelerating the reaction of adsorbed Fe(II) with O_2 at the mineral–water interface. Moses and Herman (1991) concluded that this process is in fact the rate-limiting step for pyrite oxidation at circumneutral pH. In support of this idea, at least two taxa recovered in the culture T26 metagenome (*Bradyrhizobium* and *Ralstonia*) are related to solid-phase (biotite and/or reduced smectite) Fe(II)-oxidizing organisms recently isolated from terrestrial subsoil (Shelobolina et al., 2012a) and groundwater (Benzine et al., 2013) environments where Fe redox cycling is known to be taking place. Analysis of the reconstructed genomes from culture T26 provides clues as to potential biochemical mechanisms for solid-associated Fe(II) oxidation.

4.3 | Metagenomic evidence for a Fe-based mechanism for microbial pyrite oxidation

A gene encoding a predicted outer membrane beta-barrel protein, homologous to the outer membrane cytochrome *c* (Cyc2) involved in Fe(II) oxidation by the acidophile *A. ferrooxidans* (Yarzabal et al., 2002), was found in the reconstructed *Bradyrhizobium* sp. genome (Figure 7a). Within the same gene cluster was a gene encoding a high-redox potential iron-sulfur protein (HiPIP), and three genes encoding periplasmic *c*-type cytochromes, including homologues of *A. ferrooxidans* Cyc1 and CycA1, which work together with Cyc2 to relay electrons from the outer membrane to the inner membrane for energy and NADH generation, respectively (Quatrini et al., 2009). A similar EET system involving Cyc2 and Cyc1 was also recently identified in the marine neutrophilic microaerophilic Fe(II) oxidizer *Mariprofundus ferrooxydans* PV-1 (Barco et al., 2015). Therefore, it seems feasible that the Cyc2 system in *Bradyrhizobium* sp. is involved in Fe(II) oxidation in a manner similar to Cyc2 in *A. ferrooxidans* and *M. ferrooxydans* PV-1.

In addition to cytochrome *c* that is directly embedded into the outer membrane (e.g., Cyc2), another EET mechanism involves a porin–cytochrome *c* complex (PCC), in which a periplasmic cytochrome *c* is embedded into an outer membrane porin so that the cytochrome *c* is able to access to extracellular substrates. Such a PCC genetic system (dubbed MtoAB by analogy to the MtrAB system in the dissimilatory Fe(III)-reducing bacterium Shewanella oneidensis; Shi, Rosso, Zachara, & Fredrickson, 2012) was proposed for Fe(II) oxidation by *Sideroxydans lithotrophicus* ES-1 (Liu et al., 2012) and was also identified in the reconstructed genome of related member of the *Gallionellaceae* present in the chemolithoautotrophic Fe(II)-oxidizing, nitrate-reducing culture KS (He, Tominski, Kappler, Behrens, & Roden, 2016). The clustering of genes encoding periplasmic cytochrome *c* and porin-like beta-barrel outer membrane proteins was identified in the draft genomes of *Ralstonia* sp. and *Hyphomicrobium* sp. (Figure 7b), and in the latter case the periplasmic *c*-type cytochromes contain multiple heme-binding sites. These genomic arrangements suggest that both of these taxa could have been involved in Fe(II) oxidation in a manner analogous to that suggested for *S. lithotrophicus* ES-1 and the *Gallionellaceae* sp. in culture KS.

In summary, genomic information together with the geochemical data suggest that two different biochemical mechanisms (i.e., the "indirect polythionate intermediate" and "sorbed Fe redox cycling" models; Table 2) may have played a role in microbial acceleration of pyrite oxidation in our cultures. Further experimentation will be required to assess which, if either, of the two mechanisms was the dominant one. In practice, the two pathways would be expected to operate in parallel, with the sorbed Fe redox cycling pathway likely being responsible for the main attack on the mineral surface, and the polythionate utilization pathway being responsible for oxidation of soluble, partially reduced S compounds that may arise during the reaction of pyrite surfaces with O_2 (e.g., reaction 3 in Table 2). In due course, genome-enabled (e.g., transcriptomics, proteomics) studies with pure and mixed cultures should be able to provide molecular targets (e.g., outer membrane proteins) that can be used track the presence and activity of aerobic and nitrate-reducing pyrite-oxidizing organisms in subsurface environments.

4.4 | Implications for geochemical cycling on modern and ancient Earth

4.4.1 | Modern Earth

Microbial acceleration of neutral-pH pyrite oxidation has important implications for low-temperature geochemistry in modern environments, in particular metal sulfide weathering and acid mine drainage

(AMD) systems. In such environments, acidification linked to the formation and accumulation of ferric iron during biotic and/or abiotic pyrite oxidation initiates a propagation cycle that results in massive metal sulfide leaching (Schippers, 2004). Traditionally, the early stages of AMD formation have been assumed to be kinetically slow due to the absence of high concentrations of aqueous Fe(III) at circumneutral pH (Singer & Stumm, 1970). However, our work calls for reexamination of the potential rates of pyrite oxidation in initially circumneutral-pH systems. Depending on the buffering capacity of the local surficial environment, early aerobic and/or nitrate-dependent pyrite oxidation could presumably begin the process of acidification (see net reactions in Table 2) and thereby accelerate the eventual formation of AMD conditions. A previous study of pyrite colonization and cell growth by *A. ferrooxidans* at circumneutral pH (Mielke et al., 2003) reached similar conclusions, although unlike the work presented here, that study did not directly demonstrate accelerated release of sulfate or oxidation of pyrite-Fe(II) (see Figure 1–3) during neutral-pH mineral colonization. Recent phylogenetic (16S rRNA gene) and metagenomic surveys of AMD systems with varying pH values have identified taxa that may be involved in the early stages of AMD formation under circumneutral-pH conditions (Chen et al., 2013, 2014; Korehi, Blothe, & Schippers, 2014), including neutrophilic organisms such as *T. denitrificans* with known reduced S and Fe(II) oxidation capacities (see Chen et al., 2013). Application of culture-based approaches such as those employed here could provide more direct insight into the organisms responsible for early-stage acidification in such systems.

Microbially accelerated pyrite oxidation under circumneutral-pH conditions could also play a role in the early stages of soil formation and plant establishment on arctic moraines where conglomerate rocks are rich in pyrite (Borin et al., 2010; Mapelli et al., 2011). Similarly, circumneutral-pH chemolithotrophic microbial activity has been suggested to be taking place within a ca. 1-m thick zone that exists between a low-pH surface layer and a deeper reduced zone within a black shale weathering profile in southwest China (Li et al., 2014). Microbial acceleration of neutral-pH pyrite oxidation also has implications for the geochemistry of sedimentary environments where carbonate buffering or other mineral weathering processes have the capacity to absorb protons release during pyrite oxidation, thereby maintaining neutral- or near-neutral-pH conditions (e.g., Brantley, Holleran, Jin, & Bazilevskaya, 2013; Raymond & Oh, 2009). As discussed in Bosch, Lee, Jordan, Kim, and Meckenstock (2012) and Brantley et al. (2013), attenuation of groundwater nitrate contamination, mobilization of toxic metals, and promotion of chemical weathering are all key processes likely to be impacted by pyrite oxidation in circumneutral-pH systems. From a different but highly interesting perspective, recent work by Boyd and colleagues (2014) suggests that chemolithoautotrophic pyrite oxidation drives primary productivity and mineral dissolution in a slightly alkaline (pH 8.1–8.8) subglacial environment, a process which provides an explanation for how subglacial communities could be sustained in near-isolation from the atmosphere during glacial–interglacial cycles.

4.4.2 | Early Earth

The biological acceleration of pyrite oxidation documented in this study has significant implications for the development of sulfur cycling on early Earth. Increased sulfate flux as tracked by sulfur isotopes in the late Archean has been attributed to terrestrial land colonization at 2.7–2.8 Ga (Stueken et al., 2012), at least a few hundred million years prior to the Great Oxidation Event at ca. 2.5 Ga (Kump, 2008). Increased rates of sulfate weathering flux driven by aerobic microbial pyrite oxidation could, in fact, have started as early as 2.9 Ga (Crowe et al., 2013), spurring widespread changes to geochemical cycling including impacts to the mobility of Mo, Cr, and other redox-sensitive trace metals (Konhauser et al., 2011). In addition, it is well recognized that the enhanced delivery of sulfate to the oceans which began in the late Archean ultimately had a major impact on ocean biogeochemistry (e.g., Canfield, Habicht, & Thamdrup, 2000). Although much speculation has been given to the role of low-pH, AMD-like environments in contributing to global sulfur flux on early Earth (Konhauser et al., 2011; Stueken et al., 2012), it is important to fully consider all possible sources of sulfate to the Archean ocean. Subsurface terrestrial environments rich in detrital pyrite and carbonates and receiving oxidant influx, akin to the source of sediment for these enrichment cultures would have provided sufficient shielding from destructive UV radiation on Earth's surface (Cockell, 2000; Hunting et al., 2012) to allow for sustained proliferation of circumneutral-pH lithotrophic microbial metabolism. Diffusion/dispersion together with groundwater flux would provide a mechanism for mobilizing terrestrially derived sulfate, eventually resulting in oceanic sulfate accumulation.

The recent study of neutral-pH microbially driven subglacial pyrite oxidation (Boyd et al., 2014) represents an example of this type of phenomenon. The ca. 10-fold difference between biotic and abiotic pyrite oxidation rates documented in the present study provides a concrete mechanism for biologically accelerated sulfate flux to oceans before and during the Great Oxidation Event, without the need to appeal per se to the development of widespread AMD-like conditions across the terrestrial landscape.

5 | CONCLUSIONS

Two separate enrichment cultures obtained from a terrestrial subsurface redox transition zone showed sustained sulfate generation 4-5 mmol/L, corresponding to oxidation of ca. 20% of available pyrite-S) within a month after transfer to fresh media over 12 successive transfers. Rates of pyrite oxidation were an order of magnitude higher in the presence of micro-organisms compared to abiotic controls, indicating that this microbial metabolic pathway has the potential to greatly enhance the kinetics and extent of pyrite weathering in sedimentary environments. Microbial cells were intimately associated with pyrite framboids, and microbial communities were dominated by organisms closely related to known thiosulfate and solid-phase Fe(II) oxidizers. Metagenomic analysis of one of the enrichment cultures provided insight into potential biochemical mechanisms for enhanced

pyrite oxidation, which may have proceeded through both S-related and Fe-based pathways. Our findings provide support for the hypothesized role of aerobic microbial pyrite oxidation on early Earth resulting in increased oceanic sulfate flux before and during the Great Oxidation Event. Additionally, enhanced rates of aerobic pyrite oxidation by microbial activity have direct implications for modern terrestrial environments, that is, be accelerating the early stages of AMD formation and providing the basis for a variety of chemolithotrophic microbial ecosystems. Collectively our findings call for a detailed biochemical and genetic analysis of the mechanism(s) of microbial pyrite oxidation under circumneutral-pH conditions with both O_2 and nitrate as electron acceptors.

ACKNOWLEDGMENTS

This work was supported by the NASA Astrobiology Institute; the U.S. Department of Energy, Office of Biological and Environmental Research, Subsurface Biogeochemical Research Program through the SBR Scientific Focus Area at the Pacific Northwest National Laboratory (PNNL); and by a Vilas Associateship award from the University of Wisconsin-Madison to EER. We thank J.K. Fredrickson (PNNL) for review of the manuscript, and C.M. Johnson (UW-Madison) for many fruitful discussions during the course of this research.

REFERENCES

Albertsen, M., Hugenholtz, P., Skarshewski, A., Nielsen, K. L., Tyson, G. W., & Nielsen, P. H. (2013). Genome sequences of rare, uncultured bacteria obtained by differential coverage binning of multiple metagenomes. *Nature Biotechnology*, *31*, 533–538.

Altschul, S. F., Madden, T. L., Schaffer, A. A., Zhang, J. H., Zhang, Z., Miller, W., & Lipman, D. J. (1997). Gapped BLAST and PSI-BLAST: A new generation of protein database search programs. *Nucleic Acids Research*, *25*, 3389–3402.

Ashelford, K. E., Chuzhanova, N. A., Fry, J. C., Jones, A. J., & Weightman, A. J. (2005). At least 1 in 20 16S rRNA sequence records currently held in public repositories is estimated to contain substantial anomalies. *Applied and Environment Microbiology*, *71*, 7724–7736.

Barco, R. A., Emerson, D., Sylvan, J. B., Orcutt, B. N., Meyers, M. E. J., Ramirez, G. A., … Edwards, K. J. (2015). New insight into microbial iron oxidation as revealed by the proteomic profile of an obligate iron-oxidizing chemolithoautotroph. *Applied and Environment Microbiology*, *81*, 5927–5937.

Benzine, J., Shelobolina, E., Xiong, M. Y., Kennedy, D. W., Mckinley, J. P., Lin, X., & Roden, E. E. (2013). Fe-phyllosilicate redox cycling organisms from a redox transition zone in Hanford 300 Area sediments. *Frontiers in Microbiology*, *4*, 388.

Berner, R. (1969). Synthesis of framboidal pyrite. *Economic Geology*, *64*, 383–384.

Berner, E. K., & Berner, R. A. (1996). *Global Environment: Water, Air, and Geochemical Cycles*. Upper Saddle River, NJ: Prentice Hall.

Bjornstad, B. N., Horner, J. A., Vermeul, V. R., Lanigan, D. C., & Thorne, P. D. (2009). *Borehole completion and conceptual hydrogeologic model for the IFRC well field, 300 Area, Hanford Site*. Richland, WA: Pacific Northwest Laboratory.

Blake, R., & Johnson, D. B. (2000). Phylogenetic and biochemical diversity among acidophilic bacteria that respire on iron. In D. R. Lovley (Ed.), *Environmental metal-microbe interactions* (pp. 53–78). Washington, DC: ASM Press.

Borin, S., Ventura, S., Tambone, F., Mapelli, F., Schubotz, F., Brusetti, L., … Daffonchio, D. (2010). Rock weathering creates oases of life in a High Arctic desert. *Environmental Microbiology*, *12*, 293–303.

Bosch, J., Lee, K. Y., Jordan, G., Kim, K. W., & Meckenstock, R. U. (2012). Anaerobic, nitrate-dependent oxidation of pyrite nanoparticles by *Thiobacillus denitrificans*. *Environmental Science and Technology*, *46*, 2095–2101.

Bosch, J., & Meckenstock, R. U. (2012). Rates and potential mechanism of anaerobic nitrate-dependent microbial pyrite oxidation. *Biochemical Society Transactions*, *40*, 1280–1283.

Boyd, E. S., Anbar, A. D., Miller, S., Hamilton, T. L., Lavin, M., & Peters, J. W. (2011). A late methanogen origin for molybdenum-dependent nitrogenase. *Geobiology*, *9*, 221–232.

Boyd, E. S., Hamilton, T. L., Havig, J. R., Skidmore, M. L., & Shock, E. L. (2014). Chemolithotrophic primary production in a subglacial ecosystem. *Applied and Environment Microbiology*, *80*, 6146–6153.

Boyd, E. S., Harrold, Z., & Skidmore, M. L. (2016). Contact requirements for aerobic and anaerobic pyrite oxidation by Thiobacillus denitrificans strain RG5. Unpublished data.

Brantley, S. L., Holleran, M. E., Jin, L. X., & Bazilevskaya, E. (2013). Probing deep weathering in the Shale Hills Critical Zone Observatory, Pennsylvania (USA): The hypothesis of nested chemical reaction fronts in the subsurface. *Earth Surface Processes and Landforms*, *38*, 1280–1298.

Canfield, D. E., Habicht, K. S., & Thamdrup, B. (2000). The archean sulfur cycle and the early history of atmospheric oxygen. *Science*, *288*, 658–661.

Chapelle, F. H., & Lovley, D. R. (1990). Rates of microbial metabolism in deep coastal plain aquifers. *Applied and Environment Microbiology*, *56*, 6.

Chen, Y. T., Li, J. T., Chen, L. X., Hua, Z. S., Huang, L. N., Liu, J., … Shu, W. S. (2014). Biogeochemical processes governing natural pyrite oxidation and release of acid metalliferous drainage. *Environmental Science and Technology*, *48*, 5537–5545.

Chen, L. X., Li, J. T., Chen, Y. T., Huang, L. N., Hua, Z. S., Hu, M., & Shu, W. S. (2013). Shifts in microbial community composition and function in the acidification of a lead/zinc mine tailings. *Environmental Microbiology*, *15*, 2431–2444.

Cline, J. D. (1969). Spectrophotometric determination of hydrogen sulfide in natural waters. *Limnology and Oceanography*, *14*, 454–458.

Cockell, C. S. (2000). The ultraviolet history of the terrestrial planets - implications for biological evolution. *Planetary and Space Science*, *48*, 203–214.

Crowe, S. A., Døssing, L. N., Beukes, N. J., Bau, M., Kruger, S. J., Frei, R., & Canfield, D. E. (2013). Atmospheric oxygenation three billion years ago. *Nature*, *501*, 535–538.

Dick, G. J., Andersson, A. F., Baker, B. J., Simmons, S. L., Yelton, A. P., & Banfield, J. F. (2009). Community-wide analysis of microbial genome sequence signatures. *Genome Biology*, *10*. doi:10.1186/gb-2009-10-8-r85.

Dos Santos, E. C., Silva, J. C. D., & Duarte, H. A. (2016). Pyrite oxidation mechanism by oxygen in aqueous medium. *Journal of Physical Chemistry C*, *120*, 2760–2768.

Druschel, G. K., Emerson, D., Sutka, R., Glazer, B. G., Kraiya, C., & Luther, G. W. (2008). Low oxygen and chemical kinetic constraints on the geochemical niche of neutrophilic iron(II) oxidizing microorganisms. *Geochimica et Cosmochimica Acta*, *72*, 3358–3370.

Dupont, C. L., Rusch, D. B., Yooseph, S., Lombardo, M. J., Richter, R. A., Valas, R., … Venter, J. C. (2012). Genomic insights to SAR86, an abundant and uncultivated marine bacterial lineage. *ISME Journal*, *6*, 1186–1199.

Edgar, R. C., Haas, B. J., Clemente, J. C., Quince, C., & Knight, R. (2011). UCHIME improves sensitivity and speed of chimera detection. *Bioinformatics*, *27*, 2194–2200.

Edwards, K. J., Rogers, D. R., Wirsen, C. O., & Mccollom, T. M. (2003). Isolation and characterization of novel psychrophilic, neutrophilic,

Fe-oxidizing chemolithoautotrophic α- and γ-*Proteobacteria* from the deep sea. *Environmental Microbiology*, *69*, 2906–2913.

Emerson, D., Rentz, J. A., Lilburn, T. G., Davis, R. E., Aldrich, H., Chan, C., & Moyer, C. L. (2007). A novel lineage of Proteobacteria involved in formation of marine Fe-oxidizing microbial mat communities. *PLoS ONE*, *2*, e667. doi:10.1371/journal.pone.000066.

Emerson, D., & Weiss, J. V. (2004). Bacterial iron oxidation in circumneutral freshwater habitats: Findings from the field and the laboratory. *Geomicrobiology Journal*, *21*, 405–414.

Fossing, H., & Jorgensen, B. B. (1989). Measurement of bacterial sulfate reduction in sediments: Evaluation of a single-step chromium reduction method. *Biogeochemistry*, *8*, 205–222.

Fowler, T. A., Holmes, P. R., & Crundwell, F. K. (2001). On the kinetics and mechanism of the dissolution of pyrite in the presence of *Thiobacillus ferrooxidans*. *Hydrometallurgy*, *59*, 257–270.

Friedrich, C. G., Rother, D., Bardischewsky, F., Quentmeier, A., & Fischer, J. (2001). Oxidation of reduced inorganic sulfur compounds by bacteria: Emergence of a common mechanism? *Applied and Environment Microbiology*, *67*, 2873–2882.

Gartman, A., & Luther, G. W. (2014). Oxidation of synthesized sub-micron pyrite (FeS_2) in seawater. *Geochimica et Cosmochimica Acta*, *144*, 96–108.

Hamilton, T. L., Peters, J. W., Skidmore, M. L., & Boyd, E. S. (2013). Molecular evidence for an active endogenous microbiome beneath glacial ice. *ISME Journal*, *7*, 1402–1412.

Harrold, Z. R., Skidmore, M. L., Hamilton, T. L., Desch, L., Amada, K., Vangelder, W., … Boyd, E. S. (2016). Aerobic and anaerobic thiosulfate oxidation by a cold-adapted, subglacial chemoautotroph. *Applied and Environment Microbiology*, *82*, 1486–1495.

He, S., Tominski, C., Kappler, A., Behrens, S., & Roden, E. E. (2016). Metagenomic analyses of the autotrophic Fe(II)-oxidizing, nitrate-reducing enrichment Culture KS. *Applied and Environmental Microbiology*, *82*, 2656–2668.

Hobbie, J. E., Daley, R. J., & Jasper, S. (1977). Use of nuclepore filters for counting bacteria by fluorescence microscopy. *Applied and Environment Microbiology*, *33*, 1225–1228.

Hugenholtz, P., Tyson, G. W., & Blackall, L. L. (2002). Design and evaluation of 16S rRNA-targeted oligonucleotide probes for fluorescence in situ hybridization. In M. Aquinodemuro & R. Rapley (Eds.), *Gene Probes*. Methods in Molecular Biology (pp. 29–42). Vol. 179. Totowa, NJ: Humana Press.

Hunting, E., White, C., Van Gemert, M., Mes, D., Stam, E., Kraak, M., & Admiraal, W. (2012). UV radiation and organic matter composition shape bacterial functional diversity in sediments. *Frontiers in Microbiology*, *4*. doi:10.3389/fmicb.2013.00317.

Huson, D. H., & Weber, N. (2013). Microbial Community Analysis Using MEGAN. In E. F Delong (Ed.), *Microbial Metagenomics, Metatranscriptomics, and Metaproteomics* (pp. 465–485). San Diego: Elsevier Academic Press Inc.

Kelly, D. P., & Wood, A. P. (1994). Synthesis and determination of thiosulfate and polythionates. *Methods in Enzymology*, *243*, 475–501.

Konhauser, K. O., Lalonde, S. V., Planavsky, N. J., Pecoits, E., Lyons, T. W., Mojzsis, S. J., … Bekker, A. (2011). Aerobic bacterial pyrite oxidation and acid rock drainage during the Great Oxidation Event. *Nature*, *478*, 369–374.

Korehi, H., Blothe, M., & Schippers, A. (2014). Microbial diversity at the moderate acidic stage in three different sulfidic mine tailings dumps generating acid mine drainage. *Research in Microbiology*, *165*, 713–718.

Kump, L. R. (2008). The rise of atmospheric oxygen. *Nature*, *451*, 277–278.

Li, J. W., Sun, W. M., Wang, S. M., Sun, Z. L., Lin, S. X., & Peng, X. T. (2014). Bacteria diversity, distribution and insight into their role in S and Fe biogeochemical cycling during black shale weathering. *Environ. Microb.*, *16*, 3533–3547.

Lin, X., Kennedy, D., Peacock, A., Mckinley, J., Resch, C. T., Fredrickson, J., & Konopka, A. (2012). Distribution of microbial biomass and potential for anaerobic respiration in Hanford Site 300 Area subsurface sediment. *Applied and Environment Microbiology*, *78*, 759–767.

Liu, J., Wang, Z., Belchik, S. M., Edwards, M. J., Liu, C., Kennedy, D. W., … Shi, L. (2012). Identification and characterization of MtoA: A decaheme *c*-type cytochrome of the neutrophilic Fe(II)-oxidizing bacterium *Sideroxydans lithotrophicus* ES-1. *Frontiers in Microbiology*, *3*, 37.

Lovley, D. R. (1987). Organic matter mineralization with the reduction of ferric iron: A review. *Geomicrobiology Journal*, *5*, 375–399.

Mapelli, F., Marasco, R., Rizzi, A., Baldi, F., Ventura, S., Daffonchio, D., & Borin, S. (2011). Bacterial communities involved in soil formation and plant establishment triggered by pyrite bioweathering on arctic moraines. *Microbial Ecology*, *61*, 438–447.

Markowitz, V. M., Chen, I.-M. A., Chu, K., Szeto, E., Palaniappan, K., Pillay, M., … Tringe, S. (2014). IMG/M 4 version of the integrated metagenome comparative analysis system. *Nucleic Acids Research*, *42*, D568–D573.

Mason, J., & Kelly, D. P. (1988). Thiosulfate oxidation by obligately heterotrophic bacteria. *Microbial Ecology*, *15*, 123–134.

Mielke, R. E., Pace, D. L., Porter, T., & Southam, G. (2003). A critical stage in the formation of acid mine drainage: Colonization of pyrite by *Acidithiobacillus ferrooxidans* under pH-neutral conditions. *Geobiology*, *1*, 81–90.

Mitchell, A. C., Lafreniere, M. J., Skidmore, M. L., & Boyd, E. S. (2013). Influence of bedrock mineral composition on microbial diversity in a subglacial environment. *Geology*, *41*, 855–858.

Moses, C. O., & Herman, J. S. (1991). Pyrite oxidation at circumneutral pH. *Geochimica et Cosmochimica Acta*, *55*, 471–482.

Moses, C. O., Nordstrom, D. K., Herman, J. S., & Mills, A. L. (1987). Aqueous pyrite oxidation by dissolved oxygen and by ferric iron. *Geo. et Cos Acta*, *51*, 1561–1571.

Muyzer, G., Teske, A., Wirsen, C. O., & Jannasch, H. W. (1995). Phylogenetic relationships of *Thiomicrospira* species and their identification in deep-sea hydrothermal vent samples by denaturing gradient gel electrophoresis of 16S rDNA fragments. *Archives of Microbiology*, *164*, 165–172.

Percak-Dennett, E. M., & Roden, E. E. (2014). Geochemical and microbiological responses to oxidant introduction in reduced subsurface sediment from the Hanford 300 Area, WA. *Environmental Science & Technology*, *48*, 9197–9204.

Peretyazhko, T. S., Zachara, J. M., Kukkadapu, R. K., Heald, S. M., Kutnyakov, I. V., Resch, C. T., … Moore, D. A. (2012). Pertechnetate (TcO_4^-) reduction by reactive ferrous iron forms in naturally anoxic, redox transition zone sediments from the Hanford Site, USA. *Geochimica et Cosmochimica Acta*, *92*, 48–66.

Quatrini, R., Appia-Ayme, C., Denis, Y., Jedlicki, E., Holmes, D. S., & Bonnefoy, V. (2009). Extending the models for iron and sulfur oxidation in the extreme acidophile *Acidithiobacillus ferrooxidans*. *BMC Genomics*, *10*. doi:10.1186/1471-2164-10-394.

Ravel, B., & Newville, M. (2005). ATHENA, ARTEMIS, HEPHAESTUS: Data analysis for X-ray absorption spectroscopy using IFEFFIT. *Journal of Synchrotron Radiation*, *12*, 537–541.

Raymond, P. A., & Oh, N. H. (2009). Long term changes of chemical weathering products in rivers heavily impacted from acid mine drainage: Insights on the impact of coal mining on regional and global carbon and sulfur budgets. *Earth and Planetary Science Letters*, *284*, 50–56.

Rhine, E. D., Onesios, K. M., Serfes, M. E., Reinfelder, J. R., & Young, L. Y. (2008). Arsenic transformation and mobilization from minerals by the arsenite oxidizing strain WAO. *Environmental Science and Technology*, *42*, 1423–1429.

Roden, E., Mcbeth, J. M., Blothe, M., Percak-Dennett, E. M., Fleming, E. J., Holyoke, R. R., … Emerson, D. (2012). The microbial ferrous wheel in a neutral pH groundwater seep. *Frontiers in Microbiology*, *3*, 172.

Sand, W., Gehrke, T., Jozsa, P. G., & Schippers, A. (2001). (Bio)chemistry of bacterial leaching - direct vs. indirect bioleaching. *Hydrometallurgy*, *59*, 159–175.

Schippers, A. (2004). Biogeochemistry of metal sulfide oxidation in mining environments, sediments, and soils. In: J. P. Amend, K. J. Edwards & T. W. Lyons (Eds.), *Sulfur biogeochemistry – Past and present GSA Special papers 379* (pp. 49–62). Boulder, CO: Geological Society of America.

Shelobolina, E. S., Konishi, H., Xu, H., Benzine, J., Xiong, M., Wu, T., … Roden, E. E. (2012a). Isolation of phyllosilicate–iron redox cycling microorganisms from an illite–smectite rich hydromorphic soil. *Frontiers in Microbiology*, *3*, 134.

Shelobolina, E. S., Xu, H., Konishi, H., Kukkadapu, R., Wu, T., Blothe, M., & Roden, E. E. (2012b). Microbial lithotrophic oxidation of structural Fe(II) in biotite. *Applied and Environment Microbiology*, *78*, 5746–5752.

Shi, L., Rosso, K. M., Zachara, J. M., & Fredrickson, J. K. (2012). Mtr extracellular electron transfer pathways in Fe(III)-reducing or Fe(II)-oxidizing bacteria: A genomic perspective. *Biochemical Society Transactions*, *40*, 1261–1267.

Singer, P. C., & Stumm, W. (1970). Acid mine drainage - the rate limiting step. *Science*, *167*, 1121–1123.

Sorokin, Y. I. (1970). Interrelations between sulphur and carbon turnover in meromictic lakes. *Archiv fur Hydrobiologie*, *66*, 391–446.

Sorokin, D. Y., & Lysenko, A. M. (1993). Heterotrophic bacteria from the Black Sea oxidizing reduced sulfur compounds to sulfate. *Microbiology*, *62*, 594–602.

Stegen, J. C., Konopka, A., Mckinley, J. P., Murray, C., Lin, X., & Miller, M. D. (2016). Coupling among microbial communities, biogeochemistry, and mineralogy across biogeochemical facies. *Scientific Reports*, *6*, 30553.

Stookey, L. L. (1970). Ferrozine - a new spectrophotometric reagent for iron. *Analytical Chemistry*, *42*, 779–781.

Stueken, E. E., Catling, D. C., & Buick, R. (2012). Contributions to late Archaean sulphur cycling by life on land. *Nature Geoscience*, *5*, 722–725.

Stumm, W., & Morgan, J. J. (1996). *Aquatic Chemistry*. New York: John Wiley & Sons Inc.

Sweeney, R., & Kaplan, I. (1973). Pyrite framboid formation: Laboratory synthesis and marine sediments. *Economic Geology*, *68*, 618–634.

Thauer, R. K., Jungermann, K., & Decker, K. (1977). Energy conservation in chemotropic anaerobic bacteria. *Bacteriological Reviews*, *41*, 100–180.

Trudinger, P. A. (1967). Metabolism of thiosulfate and tetrathionate by heterotrophic bacteria from soil. *Journal of Bacteriology*, *93*, 550–559.

Tuttle, J. H., Holmes, P. E., & Jannasch, H. W. (1974). Growth rate stimulation of marine Pseudomonads by thiosulfate. *Archives of Microbiology*, *99*, 1–14.

Tuttle, J. H., & Jannasch, H. W. (1972). Occurrence and types of *Thiobacillus*-like bacteria in the sea. *Limnology and Oceanography*, *17*, 532–543.

Tuttle, J. H., & Jannasch, H. W. (1976). Microbial utilization of thiosulfate in the deep sea. *Limnology and Oceanography*, *21*, 697–701.

Tuttle, J. H., & Jannasch, H. W. (1977). Thiosulfate stimulation of microbial dark assimilation of carbon dioxide in shallow marine waters. *Microbial Ecology*, *4*, 9–25.

Tuttle, J. H., & Jannasch, H. W. (1979). Microbial dark assimilation of CO_2 in the Cariaco Trench. *Limnology and Oceanography*, *24*, 746–753.

Wirsen, C. O., Brinkhoff, T., Kuever, J., Muyzer, G., Molyneaux, S., & Jannasch, H. W. (1998). Comparison of a new *Thiomicrospira* strain from the Mid-Atlantic Ridge with known hydrothermal vent isolates. *Applied and Environment Microbiology*, *64*, 4057–4059.

Wirsen, C. O., Jannasch, H. W., & Molyneaux, S. J. (1993). Chemosynthetic microbial activity at Mid-Atlantic ridge hydrothermal vent sites. *Journal of Geophysical Research: Solid Earth*, *98*, 9693–9703.

Yarzabal, A., Brasseur, G., Ratouchniak, J., Lund, K., Lemesle-Meunier, D., Demoss, J. A., & Bonnefoy, V. (2002). The high-molecular-weight cytochrome *c* Cyc2 of *Acidithiobacillus ferrooxidans* is an outer membrane protein. *FEMS Microbiology Letters*, *209*, 189–195.

Zopfi, J., Ferdelman, T. G., Jorgensen, B. B., Teske, A., & Thamdrup, B. (2001). Influence of water column dynamics on sulfide oxidation and other major biogeochemical processes in the chemocline of Mariager Fjord (Denmark). *Marine Chemistry*, *74*, 29–51.

SUPPORTING INFORMATION

Additional Supporting Information may be found online in the supporting information tab for this article.

How to cite this article: Percak-Dennett E, He S, Converse B, et al. Microbial acceleration of aerobic pyrite oxidation at circumneutral pH. *Geobiology*. 2017;00:1–14. https://doi.org/10.1111/gbi.12241